Dissociation of locomotor and cerebellar deficits in a murine Angelman syndrome model

Caroline F. Bruinsma,[1,2] Martijn Schonewille,[1] Zhenyu Gao,[1] Eleonora M.A. Aronica,[3] Matthew C. Judson,[4] Benjamin D. Philpot,[4] Freek E. Hoebeek,[1] Geeske M. van Woerden,[1,2] Chris I. De Zeeuw,[1,2,5] and Ype Elgersma[1,2]

[1]Department of Neuroscience and [2]ENCORE Expertise Centre for Neurodevelopmental Disorders, Erasmus MC, Rotterdam, Netherlands. [3]Department of (Neuro)Pathology, Academic Medical Center, Amsterdam, Netherlands. [4]Department of Cell Biology and Physiology, Neuroscience Center, and Carolina Institute for Developmental Disabilities, University of North Carolina, Chapel Hill, North Carolina, USA. [5]Netherlands Institute for Neuroscience, Royal Netherlands Academy of Arts and Sciences, Amsterdam, Netherlands.

Angelman syndrome (AS) is a severe neurological disorder that is associated with prominent movement and balance impairments that are widely considered to be due to defects of cerebellar origin. Here, using the cerebellar-specific vestibulo-ocular reflex (VOR) paradigm, we determined that cerebellar function is only mildly impaired in the *Ube3a*$^{m-/p+}$ mouse model of AS. VOR phase-reversal learning was singularly impaired in these animals and correlated with reduced tonic inhibition between Golgi cells and granule cells. Purkinje cell physiology, in contrast, was normal in AS mice as shown by synaptic plasticity and spontaneous firing properties that resembled those of controls. Accordingly, neither VOR phase-reversal learning nor locomotion was impaired following selective deletion of *Ube3a* in Purkinje cells. However, genetic normalization of αCaMKII inhibitory phosphorylation fully rescued locomotor deficits despite failing to improve cerebellar learning in AS mice, suggesting extracerebellar circuit involvement in locomotor learning. We confirmed this hypothesis through cerebellum-specific reinstatement of *Ube3a*, which ameliorated cerebellar learning deficits but did not rescue locomotor deficits. This double dissociation of locomotion and cerebellar phenotypes strongly suggests that the locomotor deficits of AS mice do not arise from impaired cerebellar cortex function. Our results provide important insights into the etiology of the motor deficits associated with AS.

Introduction

Angelman syndrome (AS) is a neurological genetic imprinting disorder caused by mutations affecting the maternally inherited *UBE3A* gene, which encodes the E3A ubiquitin protein ligase (UBE3A or E6-AP). Individuals with AS suffer from severe developmental delay, cognitive deficits, epilepsy, and a lack of speech (1). Individuals with AS also experience problems with movement and balance, an important aspect of the diagnostic criteria described in the original description of the disorder (2). Even in the least severe cases, forward lurching, unsteadiness, jerky motions, and tremulous movement of limbs may manifest (1). The locus of these motor abnormalities is currently unknown, but it is possible that cerebellar dysfunction is a causal factor, given that ataxia and tremor are both common symptoms of cerebellar disorders. In support of this hypothesis, $GABA_A$ receptors have been shown to be reduced in the cerebellum of patients with AS and in postmortem AS material (3–5). Furthermore, movement studies in patients with AS showed abnormal electromyographic (EMG) rhythmic bursts when maintaining posture (6), which could be indicative of cerebellar dysfunction. However, there has yet to be a rigorous investigation of the putative cerebellar contributions to AS motor phenotypes.

Mice that maternally inherit *Ube3a* gene deletions (AS mice, referred to herein as *Ube3a*$^{m-/p+}$ mice) are a suitable model for studying the origin of motor deficits in AS, as they exhibit globally impaired motor coordination when performing tasks on the accelerating rotarod and balance beam and in bar cross and gait tests (7–12). AS mice exhibit deficits in cerebellar granule and Purkinje cell function that are suggestive of cerebellar dysfunction (13). However, similar to the human behavioral studies, none of these motor tests conducted with mice are specific for cerebellar dysfunction; genetic, anatomic, or pharmacologic lesions in other parts of the brain are known to also affect performance on these type of tasks (14). Moreover, UBE3A is not only highly expressed in the cerebellum, but also in other sensorimotor brain structures such as the cerebral cortex and striatum (7, 8, 15–18). Hence, the observed motor deficits can just as easily arise from circuit dysfunction outside of the cerebellum as from within the cerebellum.

Here, we leveraged conditional *Ube3a* genetics and cerebellum-specific behavioral tasks to elucidate the extent to which cerebellar dysfunction is responsible for the motor deficits in AS. Despite normal Purkinje cell physiology in AS mice, we found mild cerebellar learning deficits that correlated with reductions in tonic inhibition onto granule cells. However, cerebellar learning deficits proved to be clearly dissociable from locomotor deficits when we reinstated

Note regarding evaluation of this manuscript: Manuscripts authored by scientists associated with Duke University, The University of North Carolina at Chapel Hill, Duke-NUS, and the Sanford-Burnham Medical Research Institute are handled not by members of the editorial board but rather by the science editors, who consult with selected external editors and reviewers.

Conflict of interest: The authors have declared that no conflict of interest exists.

Submitted: July 2, 2015; **Accepted:** September 10, 2015.

Reference information: *J Clin Invest*. 2015;125(11):4305–4315. doi:10.1172/JCI83541.

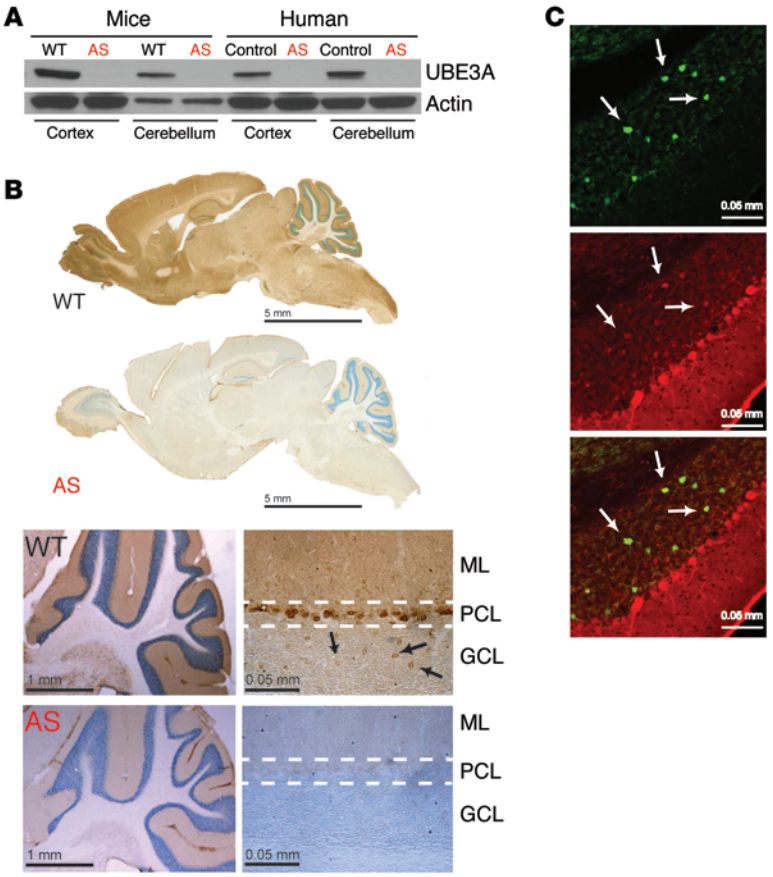

Figure 1. UBE3A is highly expressed in the cerebellum. (**A**) Western blot analysis revealed high UBE3A expression levels in the cerebellum of mice and humans. Cortical samples of the same protein concentration were used as a reference. UBE3A protein was greatly reduced in AS mice and in AS patients, indicating that UBE3A expression was almost exclusively derived from the maternal allele in cerebellar neurons. The Western blot shown is representative of samples run in duplicate. (**B**) UBE3A IHC in the cerebellum of WT mice revealed robust labeling of Purkinje cells (in the Purkinje cell layer [PCL]) and sparsely labeled cells within the molecular layer (ML). High expression levels were also observed in sparsely labeled cells in the granule cell layer (GCL) (white arrows), indicative of Golgi cell labeling. (**C**) UBE3A immunofluorescence (red, middle panel) colocalized with GlyT2-EGFP expression (green, top panel) in sparsely labeled cells in the granule cell layer, identifying them as Golgi cells. Each staining was performed using a minimum of 3 mice. Scale bars: 5 mm (**B**, top panels), 1 mm (**B**, bottom left panels), 0.05 mm (**B**, bottom right panels, and **C**).

Ube3a expression specifically in the cerebellum or following genetic normalization of CaMKII signaling. We therefore conclude that locomotor deficits in AS are most likely not of cerebellar origin.

Results

The cerebellar cortex expresses high levels of UBE3A in Purkinje and Golgi cells. Cell type–specific silencing of the paternal *Ube3a* allele dictates that UBE3A expression in neurons is solely provided by the maternal *Ube3a* allele (19–22). To determine whether cerebellar neurons are subject to similar imprinting rules, we performed Western blot analyses of UBE3A protein expression in cerebellar homogenates from WT and AS mice. Consistent with the expected effects of paternal *Ube3a* imprinting, UBE3A levels in AS cerebella were reduced to 6% ± 5% of levels in WT controls (Figure 1A). To verify that *UBE3A* is also imprinted in the human cerebellum, we extended our UBE3A Western analyses to samples obtained postmortem from individuals with AS and neurotypical controls. We found that UBE3A expression in the AS cerebellum was drastically reduced relative to that in controls, confirming that UBE3A expression in the human cerebellum is almost exclusively derived from the maternal allele (Figure 1A).

We next used immunohistochemistry (IHC) to spatially map maternal UBE3A protein expression within the cerebellum. Previous studies documented robust maternal UBE3A expression in Purkinje neurons (7, 8, 13, 15–18), which we also observed (Figure 1B). In addition, consistent with previous observations in maternal *Ube3a-YFP* reporter mice (17), we observed prominent UBE3A immunoreactivity in a subset of putative GABAergic interneurons within the granule cell layer of WT but not AS mice (Figure 1B). We subsequently confirmed their identity by colocalization with GlyT2-EGFP (Figure 1C), which specifically labels Golgi interneurons within the cerebellar granule cell layer (23). Hence, we conclude that maternal UBE3A expression in the adult cerebellar cortex is enriched in Purkinje and Golgi cells.

AS mice show only mild cerebellar learning deficits. A large body of evidence has shown that cerebellar dysfunction commonly impairs the adaptation of compensatory eye movements (24–27). This adaptation is critically important to stabilize images on the retina and prevent retinal slip. The contribution of the visual and vestibular reflex pathways can be separately quantified by providing either visual stimulation (only the screen is rotating) to trigger an optokinetic reflex (OKR) or vestibular stimulation (only the mouse is rotating) to elicit a vestibulo-ocular reflex (VOR) (for a visual explanation of these compensatory eye movement paradigms, see the cartoon in Figure 2 and ref. 28). To investigate whether AS mice showed abnormalities in gross cerebellar function, we first measured baseline OKR and VOR performance during sinusoidal visual or turntable stimulation. AS mice showed no deficits (OKR gain repeated-measures ANOVA $F_{1,12} = 0.0$, $P = 1.0$, phase $F_{1,12} = 0.0$, $P = 0.9$ and VOR gain $F_{1,12} = 4.6$, $P = 0.05$ and phase $F_{1,12} = 4.1$, $P = 0.06$) in the baseline amplitude (gain) or timing (phase) of either the optokinetic or vestibular reflex (Figure 2, A and B). In addition, we examined the visually enhanced VOR (VVOR), which uses a combination of visual and vestibular information to move

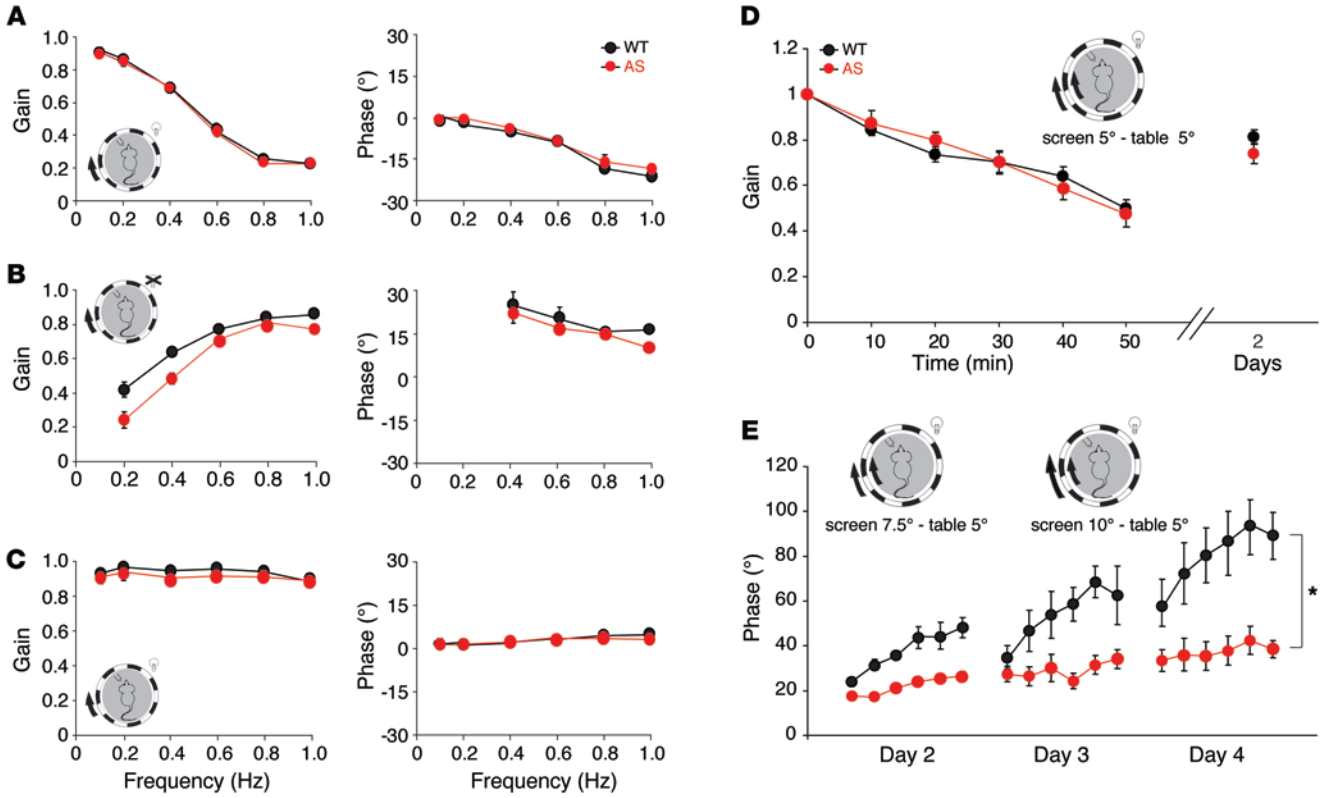

Figure 2. AS mice show only mild specific cerebellar deficits. Baseline compensatory eye movements were evaluated by recording the OKR in the light (**A**), the VOR in the dark (**B**), and the VVOR in the light (**C**) (n = 7, for both WT and AS groups in all experiments). To test the OKR, the mice were subjected to visual stimulation by sinusoidally rotating the surrounding screen with the light on (**A**). VOR responses, driven by vestibular input, were induced by rotating the table in the dark (**B**). Combining both visual and vestibular stimulation by rotating the turntable while the light was on evoked the VVOR (**C**). No differences between genotypes were observed in OKR, VOR, or VVOR with respect to gain and phase. (**D**) The adaptability of the VOR was tested with a VOR gain-decrease protocol, in which the turntable with the mouse was rotated at the same amplitude (5°) and direction as the surrounding screen. No difference was observed in the VOR gain decrease or in the consolidation of learning the next day. (**E**) Following the VOR gain-decrease protocol shown in **D**, mice were subjected to a VOR phase-reversal protocol, in which the turntable with the mouse was rotated at a 5° amplitude and the surrounding screen at a 7.5° amplitude on day 2 and at a 10° amplitude on days 3 and 4, in the same direction. AS mice were significantly impaired in this more demanding cerebellar learning task. *$P < 0.05$, as determined by repeated-measures ANOVA. Error bars indicate the SEM.

the eye. Again, the response of the VVOR was unaffected (repeated-measures ANOVA $F_{1,12} = 0.9$, $P = 0.6$ gain and $F_{1,12} = 0.0$, $P = 1.0$ phase $F_{1,12} = 0.0$, $P = 1.0$) in AS mice (Figure 2C). These results indicate that cerebellar functions subserving basic eye movement performance are not altered by a lack of UBE3A protein.

We further assessed cerebellum-dependent learning using the VOR gain-decrease adaptation test and phase-reversal paradigms. In the VOR gain-decrease test, the surrounding screen rotated in the same direction (in-phase) and with the same amplitude as the head of the animal, which was fixed to the turntable (27). There was no difference between genotypes in VOR gain-decrease learning, as neither the ability to reduce the gain (repeated-measures ANOVA $F_{3,22} = 1.6$, $P = 0.2$) nor the ability to consolidate the learned response overnight was affected (ANOVA $F_{3,22} = 2.2$, $P = 0.12$) (Figure 2D). In contrast, AS mice showed prominent deficits (repeated-measures ANOVA $F_{3,22} = 9.3$, $P < 0.0001$; all $P < 0.05$ by post-hoc test) in the VOR phase-reversal paradigm (Figure 2E), during which the visual stimulus also rotated in the same direction as the head but with greater amplitude, effectively reversing the direction of the VOR (29).

Taken together, these results show that AS mice perform normally on cerebellar tests such as the OKR, VOR, VVOR, and VOR gain-decrease paradigms, but show a striking impairment in the more demanding phase-reversal eye movement task. These results indicate the presence of mild cerebellar deficits in AS mice.

Parallel fiber–to–Purkinje cell plasticity is not affected in AS mice. Plasticity deficits at the parallel fiber (PF) to Purkinje cell synapse can result in cerebellar learning deficits (29). To investigate whether AS mice have impaired PF–Purkinje cell plasticity, we performed whole-cell recordings of Purkinje cells while inducing either long-term potentiation (LTP) via 1 Hz stimulation of PFs or long-term depression (LTD) via 1 Hz paired stimulation of PFs and climbing fibers (CFs). Both LTP and LTD could be readily induced to a similar degree in AS and WT mice (for LTP: AS 126% ± 6.4%, WT 125% ± 5.4%, $P = 0.77$; for LTD: AS 57% ± 5.3%, WT 64% ± 2.9%, $P = 0.26$) (Figure 3, A and B). In addition, paired-pulse facilitation (PPF) (with 50 ms between pulses), a measure of neurotransmitter release, was similar between AS and WT mice both before and after LTP/LTD induction (data not shown), making it unlikely that postsynaptic plasticity deficits were masked by pre-

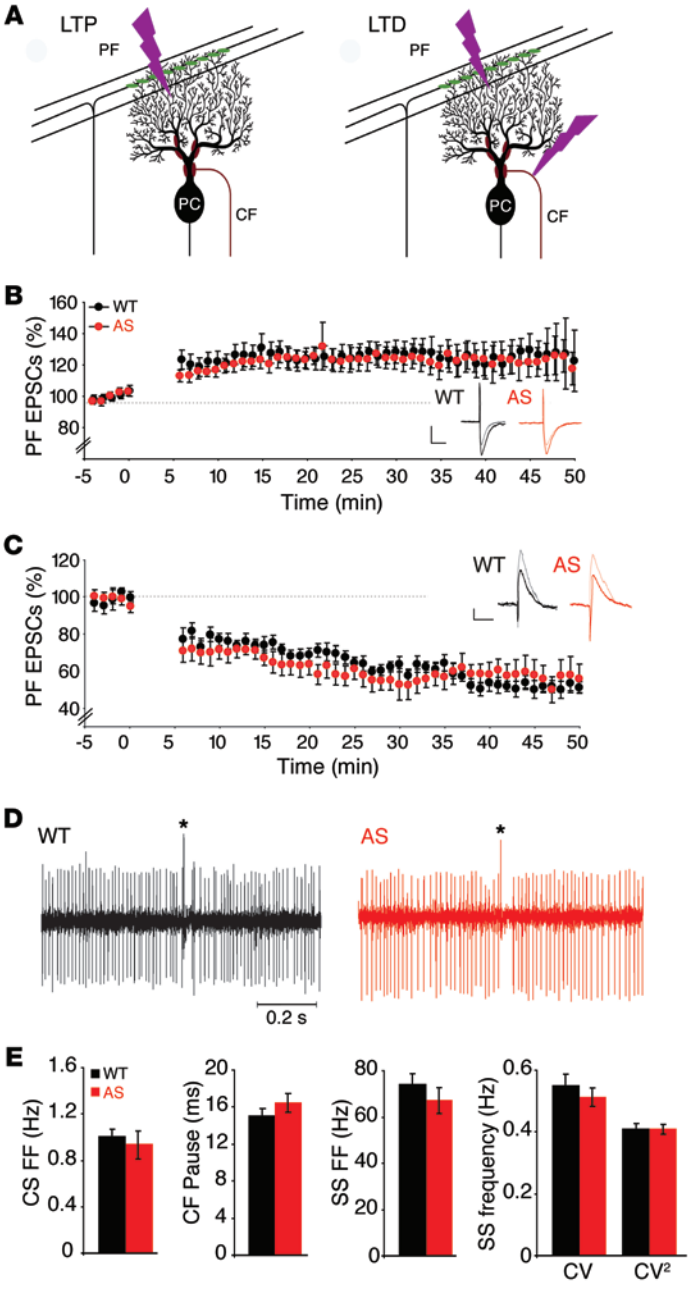

Figure 3. Normal PF–Purkinje cell plasticity and firing in AS mice. (**A**) Schematic representation of the placement of stimulus electrodes to induce LTP or LTD. PC, Purkinje cell. (**B**) LTP of the PF–Purkinje cell synapse was induced in Purkinje cells by PF stimulation at 1 Hz for 5 minutes. A repeated-measures ANOVA revealed no significant differences between the normalized EPSC amplitude in WT (n = 8) or AS mutants (n = 7) 45–50 minutes after the induction of LTP. Insets show representative traces before (bold line) and after (thin line) induction of LTP. (**C**) LTD of the PF–Purkinje cell synapse was recorded in Purkinje cells after conjunctive PF-CF stimulation at 1 Hz for 5 minutes. No difference was observed between the normalized EPSC amplitude in WT (n = 8) and AS mutants (n = 7) 45–50 minutes after the induction of LTD (assessed by repeated-measures ANOVA). Error bars indicate the SEM. Scale bars: 10 pA and 10 ms (**B** and **C**). (**D**) Representative raw traces of extracellular single-unit recordings of spontaneous activity in Purkinje cells of WT and AS mice. Asterisks indicate complex spikes. (**E**) Purkinje cell–firing analysis showed no differences (Student's 2-tailed t tests) in the complex spike (CS) firing rate, the CF pause, the simple spike (SS) firing rate, or in the CV and CV² simple spikes (n = 22 for AS and n = 19 for WT). Error bars indicate the SEM. FF, firing frequency.

synaptic compensatory mechanisms. Taken together, these experiments suggest that UBE3A is not required for plasticity at the PF–Purkinje cell synapse.

Spontaneous Purkinje cell activity is not altered in AS mice. Purkinje cells form the sole output cells of the cerebellar cortex and are capable of modifying their intrinsic frequency and regularity of firing (30–32). As such, the spiking pattern of the Purkinje cell is likely to encode information that is processed in the cerebellum, including during compensatory eye movements (26, 27, 33, 34). We therefore recorded the spontaneous spiking activity of Purkinje cells in awake AS mice and in their WT littermates (Figure 3C). However, we detected no significant between-groups difference in the simple spike firing rate (t_{39} = 0.9, P = 0.3), the complex spike firing rate (t_{39} = 0.5, P = 0.6), or the CF pause (t_{39} = –1.6, P = 0.10) (Figure 3, D and E). The coefficients of variation for simple interspike intervals, CV (t_{39} = 0.47, P = 0.5) and CV² (t_{39} = 0.0, P = 1.0), were also unchanged. Thus, in contrast to a previous report on another AS mouse model (35), we observed normal spontaneous Purkinje cell firing in AS mice.

Tonic inhibition of granule cells is reduced in AS mice. As shown in Figure 1, UBE3A is not only prominently expressed in cerebellar Purkinje cells, but also in cerebellar Golgi cells. Golgi cells provide tonic as well as phasic inhibition onto granule cells (36). Tonic and phasic inhibition are mediated by extrasynaptic, α-6–containing $GABA_A$ receptors and synaptic, γ-2–containing $GABA_A$ receptors, respectively (for review see ref. 29). Tonic inhibition of granule cells in AS mice has been shown to be impaired, perhaps due to hyperfunctional GAT1-mediated reductions in available extrasynaptic GABA (37). To confirm these findings in our AS mice, we recorded both tonic and phasic inhibition in granule cells dialyzed with a high-chloride internal solution at –70 mV. Mean tonic inhibition of AS granule cells (–17.1 ± 2.6 pA) was significantly lower than that of WT controls (–33.1 ± 5.6 pA; t_{22} = –2.7, P < 0.01) (Figure 4A). In contrast, phasic inhibition was not affected, as the frequency, amplitude, and kinetics of spontaneously occurring inhibitory postsynaptic currents (sIPSCs) in AS granule cells were comparable to that observed in WT mice (all P > 0.5) (Figure 4B). These data confirm that tonic but not phasic inhibition between Golgi cells and granule cells is selectively impaired in AS mice. Since the current behavioral phenotype in AS mice closely resembles the deficits of mouse mutants in which granule cell inhibition is specifically manipulated (38), we hypothesize that tonic Golgi cell inhibition of cerebellar granule cells may contribute to the cerebellar phase-reversal learning deficit of AS mice.

UBE3A expression in Purkinje cells is dispensable for normal cerebellar learning and locomotion. Given our collective observations in AS mice with normal Purkinje cell physiology (Figure 3) and mild cerebellar learning deficits (Figure 2), which may be linked to impaired tonic granule cell inhibition (38), we hypothesized that selective loss of UBE3A expression in Purkinje cells would contribute to neither cerebellar learning nor locomotor deficits. To investigate this, we deleted the maternal *Ube3a* gene specifically

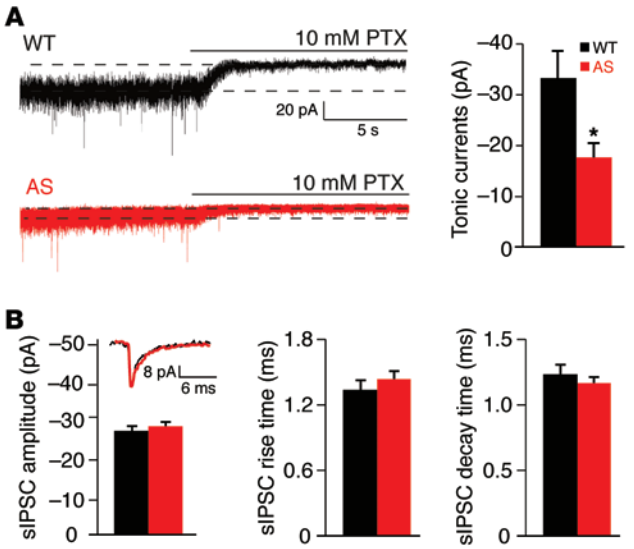

Figure 4. Reduced tonic but not phasic inhibition at the Golgi-to-granule cell synapse in AS mice. (**A**) Left: representative traces of currents recorded from 4-week-old WT and AS mouse granule cells. The amplitude of tonic currents was measured by comparing the holding currents before and after the application of picrotoxin (PTX). Right: summary of tonic currents recorded in WT (n = 10) and AS (n = 15) granule cells. Student's 2-tailed t tests showed a significant difference (*$P < 0.05$) in tonic currents. (**B**) Comparison of sIPSC amplitudes, rise times, and decay times between WT (n = 13) and AS (n = 19) mice using a 2-tailed Student's t test. Granule cells showed no changes in phasic inhibition. Error bars indicate the SEM. Inset: representative traces of sIPSCs recorded in granule cells from a 4-week-old WT mouse (black) and an AS mouse (red).

in Purkinje cells by crossing female floxed *Ube3a* mice with male mice expressing Cre recombinase from the L7 promoter (39). The resultant *Ube3a*$^{fl/p+}$ *L7-Cre* mice exhibited a selective loss of UBE3A in Purkinje neurons relative to WT (*Ube3a*$^{m+/p+}$ *L7-Cre*) controls, whereas expression in cerebellar Golgi cells remained intact (Figure 5A). We then tested whether Purkinje cell–specific deletion of UBE3A affected normal VOR phase-reversal learning. Notably, *Ube3a*$^{fl/p+}$ *L7-Cre* mice showed normal VOR phase-reversal learning and retained the ability to consolidate the learned response overnight (all $P > 0.05$), indicating that Purkinje cell–specific UBE3A loss does not affect cerebellar learning (Figure 5, C and D).

To test whether loss of UBE3A expression in Purkinje cells is responsible for the locomotor deficits, we tested *Ube3a*$^{fl/p+}$ *L7-Cre* mutant mice on the accelerating rotarod, which has reliably revealed gross motor coordination deficits in AS mice (7–12). Consistent with the observation that UBE3A expression in Purkinje cells is not required for normal cerebellar leaning, we observed no significant deficit in locomotor performance in the rotarod test (repeated-measures ANOVA $F_{1,21} = 0.7$, $P = 0.8$; Figure 5B). Hence, loss of UBE3A expression in Purkinje cells is not sufficient to cause the cerebellar and locomotor deficits observed in AS mice.

Normalization of αCaMKII inhibition rescues locomotor but not cerebellar learning deficits in AS mice. CaMKII activity is markedly reduced in AS mice, presumably due to increased inhibitory phosphorylation of αCaMKII at Thr305/Thr306 (40). Accordingly, normalizing CaMKII inhibition in AS mice by mutating the Thr305/Thr306 phosphorylation sites of the *CaMK2A* gene, thereby preventing autophosphorylation at αCaMKII Thr305 and Thr306 (41), fully restores certain capabilities, including locomotor performance (9). In the cerebellum, αCaMKII is exclusively expressed in Purkinje cells and is essential for Purkinje cell plasticity and cerebellar learning (42). Given our results showing that UBE3A expression in Purkinje cells is not required for normal cerebellar and locomotor learning, we hypothesized that introducing the αCaMKII-T305V/T306A mutation in AS mice would rescue the locomotor but not the cerebellar learning deficits. Hence, we crossed female AS (*Ube3a*$^{m-/p+}$) mutants with male heterozygous αCaMKII-TT305/6VA mutants (referred to hereafter as CaMKII-305/6VA mice). This crossing resulted in 4 genotypes (WT, AS mutants, heterozygous CaMKII-305/6VA mutants, and AS/CaMKII-305/6VA double mutants). We replicated our previous findings (43) that the AS motor deficit seen on the accelerating rotarod is rescued in the AS/CaMKII-305/6VA double mutant (repeated-measures ANOVA on genotype $F_{3,30} = 13$; $P < 0.0001$), with only AS mice showing a significant deficit in rotarod performance compared with WT mice (Figure 6A).

To investigate whether reduction of αCaMKII inhibition also rescued cerebellar function, we measured baseline OKR, VOR, and VVOR performance in the AS/CaMKII-305/6VA double mutants and control mice. Like the AS mutation, neither the CaMKII-305/6VA nor the AS/CaMKII-305/6VA double mutation affected the baseline amplitude (gain) or timing (phase) of either the optokinetic or vestibular reflex. However, whereas the AS mice again showed a clear deficit in the VOR phase-reversal paradigm, this deficit was not rescued in the AS/CaMKII-305/6VA double mutants ($F_{3,22} = 9.314$, $P < 0.0001$, by repeated-measures ANOVA), indicating that both AS mice as well as AS/CaMKII-305/6VA mice were significantly impaired compared with their littermate controls and CaMKII-305/6VA single mutants (all $P < 0.05$ by post-hoc Bonferroni test) (Figure 6, B and C). These results indicate that the molecular mechanism that underlies the VOR phase-reversal deficit is distinct from the mechanism that underlies the locomotor impairment.

Reinstatement of UBE3A expression in the cerebellum rescues cerebellar learning but not locomotor impairments. Rescue of rotarod performance in AS/CaMKII-305/6VA double mutant mice could be due to normalization of function in extracerebellar motor circuits with enriched CaMKII expression, such as in the cortex or striatum. Alternatively, gain of function in Purkinje neurons could also conceivably explain the rescue, however, this is unlikely. To further challenge the assertion of cerebellar involvement in AS motor deficits, we used *Ube3a*$^{Stop/p+}$ *Cre*$^{ERT+}$ mice (44), which, in the absence of the Cre-ERT–activating drug tamoxifen, express UBE3A at AS levels in the forebrain due to the presence of a floxed stop cassette that inhibits transcriptional read-through of the *Ube3a*^{Stop} allele. In the cerebellum, however, this inducible gene regulation system is

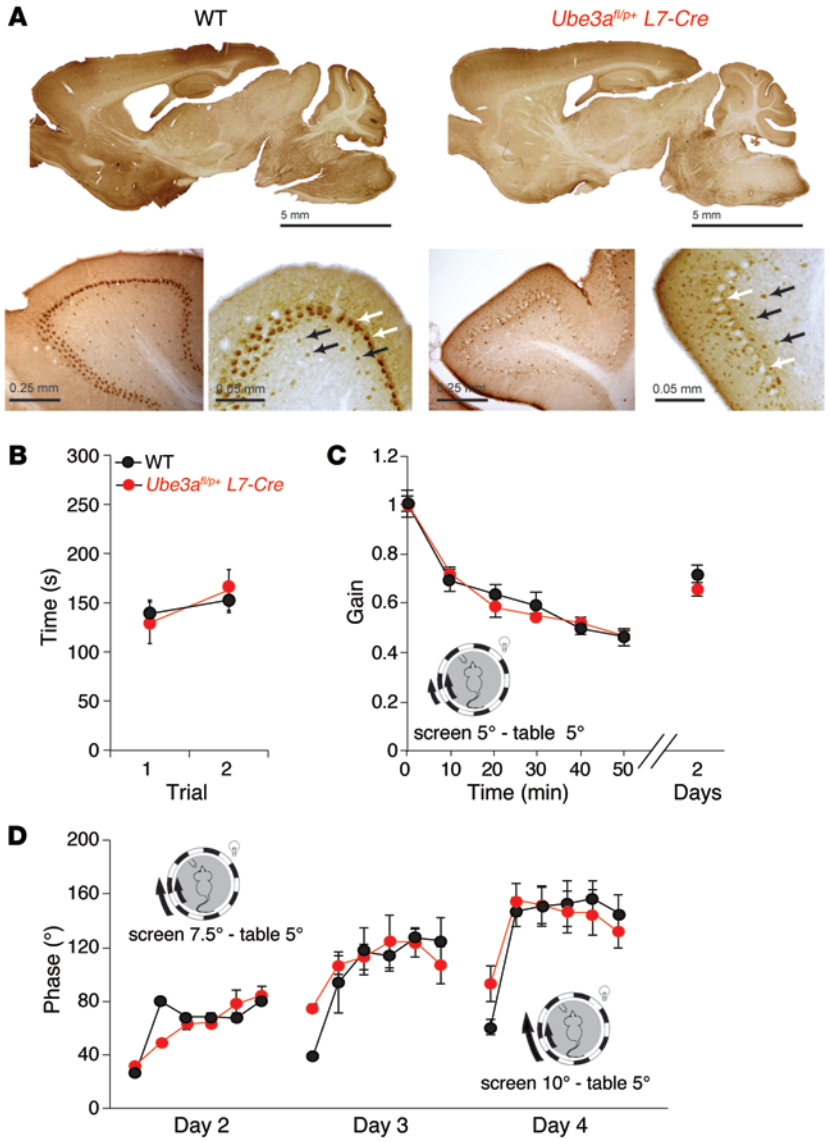

Figure 5. UBE3A expression in Purkinje cells is dispensable for normal cerebellar learning and locomotion. (**A**) IHC staining showing Purkinje cell–specific deletion of UBE3A expression in *Ube3a*$^{fl/p+}$ *L7-Cre* mice. Black arrows indicate granule cells, and white arrows indicate Purkinje cells (representative image from 3 animals). Scale bars: 5 mm (top panels), 0.25 mm (WT, bottom left; *Ube3a*$^{fl/p+}$ *L7-Cre*, bottom left) 0.05 mm (WT, bottom right; *Ube3a*$^{fl/p+}$ *L7-Cre*, bottom right). (**B**) Rotarod learning for *Ube3a*$^{fl/p+}$ *L7-Cre* (n = 10) mice was not impaired compared with that for *Ube3a*$^{m+/p+}$ *L7-Cre* (WT) (n = 10) control mice (repeated-measures ANOVA). The y axis indicates the time the mice stayed on the rotarod before falling off. (**C**) *Ube3a*$^{fl/p+}$ *L7-Cre* mice (n = 7) showed normal adaptation in the VOR gain-decrease paradigm compared with their WT littermates (n = 6). (**D**) *Ube3a*$^{fl/p+}$ *L7-Cre* mice (n = 7) showed no differences in subsequent VOR phase-reversal learning compared with control mice (n = 6). Statistical significance was tested using a repeated-measures ANOVA. Error bars indicate the SEM.

less tightly controlled, resulting in region-specific Cre recombination and reinstatement of UBE3A; *Ube3a*$^{Stop/p+}$ *Cre*$^{ERT+}$ mice express UBE3A at nearly 35% of WT UBE3A levels in the cerebellum, presumably due to leaky, tamoxifen-independent translocation of Cre-ERT to the nucleus in cerebellar neurons of this *Cag-Cre*^{ERT} line (44). Locomotor deficits in *Ube3a*$^{Stop/p+}$ *Cre*$^{ERT+}$ and AS mice were similar ($F_{1,27}$ = 39.5, P < 0.0001) (Figure 7A and ref. 44), indicating a lack of rescue by cerebellar UBE3A reinstatement. In contrast, this level of UBE3A expression proved sufficient to support normal cerebellar learning, as *Ube3a*$^{Stop/p+}$ *Cre*$^{ERT+}$ mice showed no deficits in the VOR phase-reversal learning paradigm compared with *Ube3a*$^{m+/p+}$ *Cre*$^{ERT+}$ controls (all P > 0.05; Figure 7, B and C). These results suggest that cerebellar learning deficits and locomotor impairments in AS mice are dissociable, differentially resulting from UBE3A loss in cerebellar and extracerebellar circuits, respectively.

Discussion

Patients with AS show various severities of motor deficits such as an ataxic-like gait, forward lurching, unsteadiness, clumsiness, jerky motions, and/or tremulous movement of limbs (1). The AS mouse model appears to be a suitable model for studying the motor deficits in AS, as it exhibits globally impaired motor coordination in a variety of tasks such as accelerating rotarod, balance beam, bar cross, and gait tests (7–12).

The idea that cerebellar deficits underlie the movement deficits in individuals with AS has been dogmatic since the original publication describing AS (2). Given that Purkinje cells provide the sole output of the cerebellar cortex and that these cells express high levels of UBE3A, it is also not surprising that deficient Purkinje cell function is generally believed to underlie the locomotor deficits in AS mice and in patients with AS (13). Our results in AS mice overturn both of these dogmas. First, although we show that the *Ube3a* gene is highly expressed in cerebellar Golgi and Purkinje cells and that this expression is almost exclusively derived from the maternal allele, we found that cerebellar deficits of AS mice were rather mild and were only observed with an extremely demanding cerebellar task. Second, we observed none of the changes in Purkinje cell physiology (synaptic plasticity, action potential firing) that typically correlate with cerebellar learning impairments (29). Third, we show that deletion of *Ube3a* from Purkinje cells does not affect cerebellar learning or locomotion. And last, we used several mouse models to demonstrate a double dissociation between locomotor function and cerebellar learning, which strongly argues against cerebellar dysfunction being the underlying reason for the locomotor deficits.

Consistent with previous findings (37) and the potent tonic inhibition of granule cell activity by Golgi cell inhibition, we observed impaired tonic inhibition of granule cells by Golgi cells in AS mice. The moderate behavioral cerebellar phenotype in AS mice is in line with impaired granule cell inhibition, as similar phenotypes have been observed in other mouse models in which the granule cell network is specifically disrupted (ref. 45 and for review

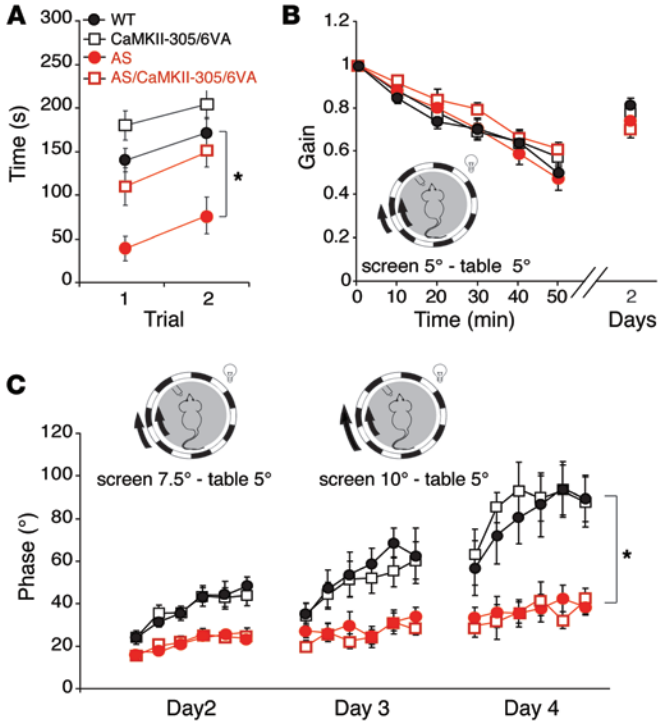

Figure 6. Reduction of αCaMKII inhibition rescues motor performance on the rotarod but not cerebellar learning. (**A**) Rotarod learning in AS mice was impaired and could be rescued by reducing αCaMKII inhibition through the αCaMKII-305/6VA mutation. The *y* axis indicates the time the mice stayed on the rotarod before falling off (WT, $n = 10$; AS, $n = 7$; CaMKII-305/6VA, $n = 10$; AS/CaMKII-305/6VA, $n = 8$). (**B**) VOR gain decrease was normal in AS and AS/CaMKII-305/6VA double mutants. Graph shows the gain decrease during a 50-minute training period on day 1 as well as the consolidation of learning on day 2. (**C**) The impaired cerebellum-dependent learning in AS mice identified by the VOR phase-reversal task could not be rescued by normalization of αCaMKII inhibition. We used 6 αCaMKII-305/6VA mutants and 7 mice each for all other genotypes. $^*P < 0.05$, as determined by a repeated-measures ANOVA, followed by a post-hoc Bonferroni test. Error bars indicate the SEM.

see ref. 29). In particular, the deficits observed in AS mice are strikingly similar to those identified in a recently reported mouse mutant with a granule cell–specific mutation in the *KCC2* KCl cotransporter gene; this genetic manipulation depolarizes granule cells by increasing their cytosolic chloride concentration. Like AS mice, these mutants also show severely impaired phase-reversal learning, while their OKR, VOR, and VVOR basic motor performance and gain-decrease learning are unaffected (38). Together, these findings suggest that defective Golgi cell functioning might contribute to the observed cerebellar phase-reversal learning deficits in AS mice. However, we also cannot rule out the possibility that the cerebellar cortex plays no role at all and that these deficits arise instead from deficits in the cerebellar nuclei.

It seems unlikely that the impaired tonic inhibition of Golgi cells onto granule cells underlies the locomotor deficits in AS mice, as ablation of cerebellar Golgi cells causes only a transient ataxia (46). Instead, the locomotor and cerebellar VOR phase-reversal deficits are likely regulated by distinct mechanisms, a hypothesis supported by our measurements of the AS/CaMKII-305/6VA–double-mutant mice. We took advantage of the fact that AS mice have reduced CaMKII activity, presumably due to increased inhibitory phosphorylation of αCaMKII T305/T306 (40), and that genetic normalization of CaMKII function in AS mice can restore rotarod motor performance (9). In the current study, we replicated this phenotype and further showed that, despite normal performance on the rotarod, AS/CaMKII-305/6VA double mutants still showed marked impairments in the VOR phase-reversal adaptation task. Notably, αCaMKII is not expressed in cerebellar nuclei nor in cerebellar Golgi cells, which excludes the possibility that the rescue of the locomotor phenotype arises from impaired αCaMKII signaling in these cells (42). In separate experiments, we showed that reinstatement of UBE3A in the cerebellum could rescue the cerebellar VOR phase-reversal learning deficit, but not the rotarod deficit. These results provide further evidence that the VOR phase-reversal learning and rotarod deficits in AS mice arise through distinct mechanisms.

Collectively, our findings suggest that the mild cerebellar deficits of AS mice are not responsible for their pronounced locomotor deficits. Other candidate brain areas that could contribute to these locomotor deficits are the motor cortex and the nigrostriatal pathway, in which both UBE3A and αCaMKII are highly expressed. Notably, a recent study showed that AS mice exhibited behavioral deficits that correlated with abnormal dopamine signaling (47). Specifically, AS mice exhibited changes in dopamine release in both the mesolimbic and nigrostriatal pathways (47), whereas another study reported increased dopamine levels in the striatum, midbrain, and frontal cortex of AS mice (48). AS mice were also shown to have a reduced number of tyrosine hydroxylase–positive neurons in the substantia nigra (10). Interestingly, CaMKII phosphorylation is increased in the striatum of AS mutant mice (10), and CaMKII has been shown to be a regulator of the dopamine transporter and the dopamine D3 receptor (49–51). Collectively, these findings could indicate that impaired CaMKII/dopamine signaling in the nigrostriatal pathway is a possible mechanism underlying the AS motor pathophysiology. This issue remains to be addressed in future studies.

In conclusion, we show here that AS mice have rather mild cerebellar deficits and that these deficits are likely caused by the impaired tonic inhibition of granule cells rather than by Purkinje cell dysfunction. Moreover, we show through genetic manipulations that there is a double dissociation between cerebellar deficits and locomotor deficits, such that we can correct locomotor learning without rescuing cerebellar learning, and vice versa. These results strongly suggest that the cerebellar cortex plays a minor role at best in the pronounced motor performance deficits observed in AS mice.

Methods

Mice. Mutant mice harboring the *Ube3a*-null mutation (referred to herein as AS mice) and mutants heterozygous for the targeted *αCaMKII-T305V/T306A* mutation, which prevents phosphorylation at these residues (referred to herein as CaMKII-305/6VA mice), were developed as described previously (7, 9, 41). Mutant $Ube3a^{Stop/p+}$ mice were developed as described previously (44). $Ube3a^{fl/p+}$ mice were generated at the University of North Carolina Animal Models Core facility by using the

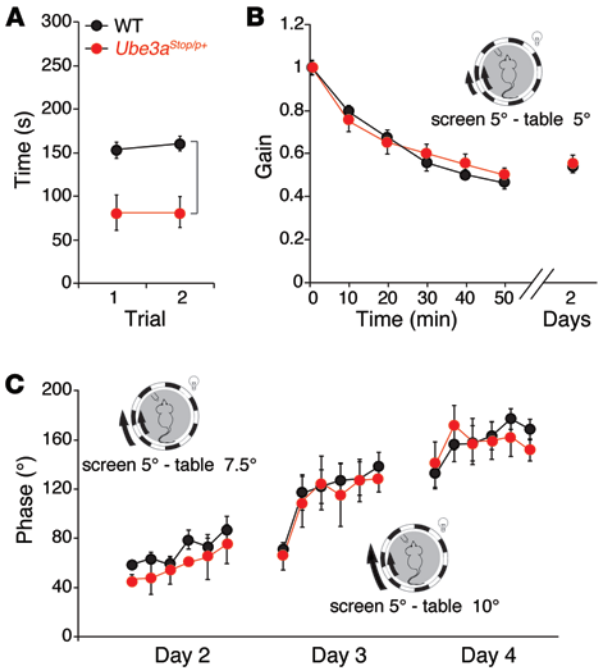

Figure 7. Cerebellar reinstatement of UBE3A expression rescues cerebellar learning but not rotarod learning. (**A**) Rotarod learning for *Ube3a*$^{Stop/p+}$ *Cre*$^{ERT+}$ mice was impaired compared with that of *Ube3a*$^{m+/p+}$ *Cre*$^{ERT+}$ control (WT) mice. The *y* axis indicates the time the mice stayed on the rotarod before falling off. (**B**) VOR gain decrease for *Ube3a*$^{Stop/p+}$ *Cre*$^{ERT+}$ and control (WT) mice during a 50-minute training period on day 1 as well as the consolidation test on day 2. No differences were observed between the genotypes. (**C**) *Ube3a*$^{Stop/p+}$ *Cre*$^{ERT+}$ mice showed no differences in VOR phase-reversal learning compared with control (WT) mice. Following the VOR gain decrease shown in **B**, the mice were further trained by rotating them at a 5° amplitude while the surrounding screen was rotated at a 7.5° amplitude (day 2) and a 10° amplitude (days 3 and 4), in the same direction, to induce VOR phase reversal. For all experiments, 7 mice of each genotype were used. *$P < 0.05$, as determined by a repeated-measures ANOVA, followed by a post-hoc Bonferroni test. Error bars indicate the SEM.

Ube3a^{KO1st} targeting construct (CSD46841; clone PG00126_Z_3_B08 A1), generated by the trans-NIH Knockout Mouse Project (KOMP; www.komp.org). Targeted C57BL/6N-tac mouse embryonic stem cells (PRX-B6N 1; Primogenix) were used to derive chimeric *Ube3a*^{KO1st} males, which were crossed with C57BL/6 *Rosa26-FLPe* mice (009086; The Jackson Laboratory) to excise the *FRT*-flanked lacZ gene trap from the *Ube3a*^{KO1st} allele, resulting in the conditional *Ube3a* floxed allele (*Ube3a*$^{fl/+}$). The *FLPe* allele was eliminated by further crossing the mice on a congenic C57BL/6 background (000664; The Jackson Laboratory), on which the line was maintained. The GlyT2-EGFP was generated and provided by J.M. Fritschy (University of Erlangen-Nuremberg, Erlangen, Germany) (23). With the exception of the experiments using the *Ube3a*$^{fl/p+}$ mice, all experiments described in this article were carried out using hybrid mice on a F1 129/Sv-C57BL/6 background, with the mutant *Ube3a* allele coming from the female mice on a 129/Sv background. Experiments using the *Ube3a*$^{fl/p+}$ mice were performed on the C57BL/6 background. Mouse pups were genotyped at P5 to P7 and then coded to facilitate blinded analyses. Animals were re-genotyped after the completion of all experiments, and the code was broken only prior to performing the final statistical analyses.

IHC. Mice were anesthetized by i.p. injection of pentobarbital and perfused with saline, followed by 4% paraformaldehyde. Mice were dissected and the brains removed and treated for another 2 hours in 4% paraformaldehyde at 4°C. Subsequently, the brains were transferred into 30% sucrose solution and kept overnight at 4°C. Using a freezing microtome (SM 2000R; Leica), 40-μm sagittal sections were collected in 0.1 M phosphate buffer (PB). Sections were preincubated in sodium citrate (10 mM) at 80°C for 1 hour, rinsed with TBS (pH 7.6), and treated with 0.4% Triton X-100 and 10% normal horse serum (Invitrogen) in TBS buffer for 1 hour at room temperature. Sections were incubated with monoclonal E6AP antibody (clone 330; Sigma-Aldrich) and diluted 1:500 in TBS buffer with 0.4% Triton X-100 and 2% normal horse serum for 72 hours at 4°C. Postincubation sections were washed using TBS and incubated with secondary Cy3 antibody (Jackson ImmunoResearch; ALG 715-165-150) and diluted 1:200 in TBS buffer with 0.4% Triton X-100 and 2% normal horse serum for 2 hours at room temperature. Sections were then washed with 0.1 M PB and mounted and covered using VECTASHIELD H1000 (Vector Laboratories). Images were captured using a Zeiss LSM 700 confocal microscope (Carl Zeiss) equipped with Zeiss Plan-Apochromat ×10/0.45, ×20/0.8 (both air), and ×40/1.3 (oil immersion) objectives. GFP and Cy3 were imaged using excitation wavelengths of 488 and 550 nm, respectively.

For DAB staining, brains were fixed with 4% paraformaldehyde by transcardial perfusion, as described above. Immunocytochemistry was performed on free-floating 40-μm frozen sections using a standard avidin-biotin-immunoperoxidase complex (ABC) method (Vector Laboratories) with anti-E6AP (1:1,000; clone E6AP-330; Sigma-Aldrich) as the primary antibody and rabbit anti-mouse HRP as the secondary antibody (1:200; ALG P0260; Dako), followed by DAB staining.

Western blot analysis. For measurement of UBE3A protein expression, mice were sacrificed by cervical dislocation, and the cerebellum was snap-frozen in liquid nitrogen. Human temporal cortex tissue was obtained from the National Institute of Child Health and Human Development (NICHD) Brain and Tissue Bank for Developmental Disorders. The tissues were homogenized in a lysis buffer containing 10 mM Tris-HCl (pH 6.8), 2.5% SDS, 2 mM EDTA, and a protease and phosphatase inhibitor cocktail (Sigma-Aldrich). Fifteen micrograms of protein was used for Western blot analyses. The Western blots were probed with an antibody against UBE3A (1:5,000; BD Transduction Laboratories) and actin (1:10,000; Chemicon). The bands were visualized using ECL (Pierce, Thermo Fisher Scientific). For quantification of protein levels, gray scale values of pixels of the UBE3A bands were calculated and corrected for the actin levels using ImageJ software (NIH).

Behavioral analysis. Mice were housed in groups of 2 to 4 mice per home cage. Genotype groups were age and sex matched. The mice were kept on a 12-hour light/12-hour dark cycle, with ad libitum access to food and water. Behavioral experiments were performed during the light period of the cycle by a person who was blinded to the genotype.

Rotarod. Motor coordination of 3- to 4-month-old mutant mice and their WT littermates was tested on an accelerating rotarod (model 7650, Ugo Basile; Biological Research Apparatus). Performance was determined as the average of 2 trials with an inter-training interval of 1 hour. This was repeated for 2 to 5 days. The rotarod has a cylinder with a diameter of 3 cm that can accelerate from 4 to 40 rpm in 300 seconds. The latency to stay on the rotarod was recorded by determining the time taken for a mouse to drop off or stop running for 3 consecutive rotations.

Eye movement recordings. Compensatory eye movements were recorded as described before (28). In short, mice were anesthetized, and an immobilizing construction containing 2 attached nuts (3 mm each) was placed on the frontal and parietal bones using OptiBond primer and adhesive (Kerr) and Charisma (Heraeus Kulzer). After 5 days of recovery, mice were head fixed and placed in a restrainer in the middle of a turntable surrounded by a cylindrical screen (with a diameter of 60 and 63 cm, respectively). After a habituation session, baseline OKR, VOR, and VVOR were evoked by rotating the screen and/or table (5° amplitude, 0.1–1.0 Hz frequency). The next day, mice were subjected to five 10-minute periods of sinusoidal in-phase screen and table rotations (both at 5° amplitude, 0.6 Hz) aimed at decreasing the gain of the VOR. On the subsequent days, the VOR was phase reversed by five 10-minute periods of in-phase table and screen rotations at 0.6 Hz, with screen amplitudes varying from 7.5° (day 2) to 10° (days 3 and 4). Mice were kept in the dark between training days to prevent active extinction. Before, between, and at the end of each training session, the VOR was measured. Mice used for eye movement recordings were littermates between 3 and 6 months of age (average age of 21 weeks for WT mice, 22 weeks for AS mice, 24 weeks for CaMKII-305/6VA mice, and 23 weeks for CaMKII-305/6VA AS mutants; not statistically different; 1-way ANOVA $F_{3,22} = 9.2$, $P = 0.6$). The eye movements were recorded at 240 Hz using a CCD camera fixed to the table, and pupil position was obtained using an eye-tracking system (ISCAN). Video calibrations and subsequent eye movement computations were performed with custom-made MATLAB (MathWorks) routines, as described previously (33). To analyze compensatory eye movements, phase and gain were calculated by fitting a sine function to the averaged eye and stimulus velocity traces. Gain was calculated as the ratio of eye-to-stimulus velocity traces. Phase was computed as the difference in degrees between the eye and the stimulus velocity.

In vitro electrophysiology. For in vitro recordings of Purkinje cells, cerebellar slices were prepared according to a standardized protocol to allow recordings of long-term synaptic plasticity at the PF–Purkinje cell synapse (43). Slices of the cerebellar vermis (250 μm) from 10- to 30-week-old mice were obtained by decapitation after isoflurane anesthesia. Slices were cut in ice-cold oxygenated (with 95% O_2 and 5% CO_2) solution containing 240 mM sucrose, 5 mM KCl, 1.25 mM Na_2HPO_4, 2 mM $MgSO_4$, 1 mM $CaCl_2$, 26 mM $NaHCO_3$, and 10 mM D-glucose. Next, slices were transferred to a submerged room-temperature holding chamber with artificial cerebral spinal fluid (ACSF) containing 124 mM NaCl, 5 mM KCl, 1.25 mM Na_2HPO_4, 2 mM $MgSO_4$, 2 mM $CaCl_2$, 26 mM $NaHCO_3$, and 15 mM D-glucose oxygenated with 95% O_2 and 5% CO_2. Purkinje cells were visualized using a standard upright microscope (Zeiss) and recorded using an EPC-9 amplifier (HEKA). The resistances of the pipettes ranged from 3 to 4 MΩ when filled with intracellular solution containing 120 mM K-gluconate, 9 mM KCl, 10 mM KOH, 3.48 mM $MgCl_2$, 4 mM NaCl, 10 mM HEPES, 4 mM Na_2ATP, 0.4 mM Na_3GTP, and 17.5 mM sucrose (pH 7.25). The holding potentials ranged from –65 to –70 mV by somatic current injections between 0 and –300 pA. Throughout the recordings, series and input resistances were monitored in voltage clamp mode by a –10 mV voltage step 1 second after each stimulus, which was presented at 0.1 Hz. Recordings that showed a deviation of greater than 15 % in holding current, series, or input resistances or in paired-pulse ratios were discarded (43). Following the recording of a stable baseline of more than 10 minutes, long-term plasticity at the PF–Purkinje cell synapse was induced in current clamp mode by either pairing PF and CF stimulation at 1 Hz for 5 minutes (PF-LTD protocol) at a near-physiological temperature (34°C ± 1°C) or by PF stimulation at 1 Hz for 5 minutes at room temperature (PF-LTP protocol). For PF stimulation, ACSF-filled patch pipettes were placed in the outer third of the molecular layer laterally to the presumed position of the Purkinje cell dendritic tree to avoid direct depolarization. For CF stimulation, similar pipettes were placed in the top part of the granule cell layer near the patched Purkinje cell. Great care was taken to avoid direct depolarization of the Purkinje cell axon, which would inevitably result in a noticeable back-propagating action potential. For both stimuli, 500- to 700-μs block pulses of 1 to 10 μA were used. The stimulus strength for PF stimulation was adapted to evoke excitatory postsynaptic currents (EPSCs) of approximately 200 to 300 μA during baseline; for CF stimulation, we aimed to evoke a single CF stimulus. All patch experiments were performed in the presence of bath-applied picrotoxin (10 mM) to block inhibitory transmission, unless stated otherwise. All chemicals were purchased from Sigma-Aldrich. For statistical analysis, the last 5 minutes of the traces were used.

Granule cell recordings were done as described above, but we used P30–P32 animals and kept the slices in ACSF for more than 1 hour at 34°C ± 1°C before the experiments started. In addition, granule cells were recorded using patch pipettes of 5 to 7 MΩ filled with intracellular solution containing 150 mM CsCl, 15 mM CsOH, 1.5 mM $MgCl_2$, 0.5 mM EGTA, 10 mM HEPES, 4 mM Na_2ATP, and 0.4 mM Na_3GTP (pH 7.3). Recordings were performed at 34°C using standard ACSF supplemented with 10 μM NBQX and 10 μM D-AP5. Granule cells were held at –70 mV (without junction potential correction) in voltage clamp configuration. Recordings during which the initial holding current increased over –100 pA and/or the series resistance increased over 25 MΩ were excluded from analysis. The tonic $GABA_A$ receptor–mediated current was measured by comparing the difference in holding current recorded in the presence and absence of 10 mM picrotoxin. sIPSCs were detected using the Mini Analysis program (Synaptosoft). Cutoff amplitudes for IPSC detection were set at 6 to 8 pA. All selected IPSCs were visually inspected. Averaged IPSC waveforms were constructed exclusively from nonoverlapping events. The decay time was calculated as the time from the peak to 37% of the peak amplitude.

In vivo electrophysiology. A craniotomy of 2 mm was made in the left occipital bone, and a recording chamber was placed around it, allowing chronic in vivo electrophysiological recordings (52). Mice were head fixed, and extracellular Purkinje cell activity was recorded and analyzed as previously described (53). Purkinje cells were identified by the firing of complex spikes and were confirmed to be from a single unit by the presence of a pause of at least 5 ms in simple spike firing after each complex spike. The recordings were processed by a custom-made MATLAB routine based on principal component analysis. For each cell, the mean firing rate and coefficients of variation (CV and CV2) were determined for simple and complex spikes. CV is a measure of the reg-

ularity of spiking during the entire recording period and is calculated by dividing the standard deviation by the mean of all interspike intervals in a given recording; CV2 is a measure of the regularity on a spike-to-spike basis and is calculated as the mean of 2 times the difference between 2 consecutive interspike intervals (ISIs) divided by the sum of the 2 intervals, i.e., $[(2 \mid \mathrm{ISI}\,(\mathrm{ISI})_{n+1} - \mathrm{ISI}_n \mid)/(\mathrm{ISI}_{n+1} + \mathrm{ISI}_n)]$.

Statistics. For the consolidation measurement, a 1-way ANOVA test was used, followed, when significant, by a post-hoc Bonferroni test. Student's 2-tailed *t* tests were used for group comparisons of a single variable (e.g., protein levels, LTP, and LTD). A repeated-measures ANOVA with genotype as the between-subjects factor and frequency or time as the within-subjects factor was used to assess group differences in the eye movement recordings. Genotypic differences were probed with post-hoc Bonferroni comparisons. For all analyses, a *P* value of less than 0.05 was considered significant.

Study approval. All animal experiments were approved by the Dutch Dierexperimenten commissie (DEC) ethics committee and were performed in accordance with Dutch animal care and use laws.

Author contributions

CFB, CZ, and YE designed the research studies; CFB, GMW, and ZG conducted the experiments; EMAA provided human samples; BDP and MCJ generated the floxed UBE3A mice; CFB, FEH, MS, and ZG analyzed the data. All authors had significant input in the scientific discussions and writing of the manuscript.

Acknowledgments

We thank M. Elgersma, M. Aghadavoud, L. Post, R. de Avila Freire, J. Harkonen, E. Galliano, and E. Goedknegt for their technical assistance. This work was supported by grants from the Nina Foundation (to C.F. Bruinsma); the Associazione Angelman Onlus (to Y. Elgersma); the Dutch Organization for Medical Sciences (ZonMw; to C.I. De Zeeuw and Y. Elgersma); Earth and Life Sciences (ALW, to M. Schonewille, F.E. Hoebeek, and C.I. De Zeeuw). Support was also provided by Erasmus University fellowships (to G.M. van Woerden, M. Schonewille, and F.E. Hoebeek); Senter (NeuroBasic, to C.I. De Zeeuw and Y. Elgersma); European Research Council (ERC) Advanced Grants (to C.I. De Zeeuw); the Angelman Syndrome Foundation (ASF) (to B.D. Philpot and Y. Elgersma); the Simons Foundation (SFARI 274426, to B.D. Philpot and 275234, to Y. Elgersma); the NIH (R01NS085093, to B.D. Philpot and F32NS077686, to M.C. Judson); and the National Association for Research on Schizophrenia and Depression (NARSAD) (to M.C. Judson). Human cerebral and cerebellar tissue was obtained from the NICHD Brain and Tissue Bank for Developmental Disorders of the University of Maryland.

Address correspondence to: Chris I. De Zeeuw or Ype Elgersma, Department of Neuroscience, Erasmus MC, Wytemaweg 80, 3015 CN, Netherlands. E-mail: y.elgersma@erasmusmc.nl (Y. Elgersma), c.dezeeuw@erasmusmc.nl (C.I. De Zeeuw).

1. Williams CA, et al. Angelman syndrome 2005: updated consensus for diagnostic criteria. *Am J Med Genet A*. 2006;140(5):413–418.
2. Angelman H. 'Puppet' children. A report on three cases. *Dev Med Child Neurol*. 1965;7(6):681–688.
3. Odano I, et al. Decrease in benzodiazepine receptor binding in a patient with Angelman syndrome detected by iodine-123 iomazenil and single-photon emission tomography. *Eur J Nucl Med*. 1996;23(5):598–604.
4. Holopainen IE, et al. Decreased binding of [11C] flumazenil in Angelman syndrome patients with GABA(A) receptor β3 subunit deletions. *Ann Neurol*. 2001;49(1):110–113.
5. Asahina N, Shiga T, Egawa K, Shiraishi H, Kohsaka S, Saitoh S. [(11)C]flumazenil positron emission tomography analyses of brain gamma-aminobutyric acid type A receptors in Angelman syndrome. *J Pediatr*. 2008;152(4):546–549.
6. Dan B, Cheron G. Postural rhythmic muscle bursting activity in Angelman syndrome. *Brain Dev*. 2004;26(6):389–393.
7. Jiang YH, et al. Mutation of the Angelman ubiquitin ligase in mice causes increased cytoplasmic p53 and deficits of contextual learning and long-term potentiation. *Neuron*. 1998;21(4):799–811.
8. Miura K, et al. Neurobehavioral and electroencephalographic abnormalities in Ube3a maternal-deficient mice. *Neurobiol Dis*. 2002;9(2):149–159.
9. van Woerden GM, et al. Rescue of neurological deficits in a mouse model for Angelman syndrome by reduction of αCaMKII inhibitory phosphorylation. *Nat Neurosci*. 2007;10(3):280–282.
10. Mulherkar SA, Jana NR. Loss of dopaminergic neurons and resulting behavioural deficits in mouse model of Angelman syndrome. *Neurobiol Dis*. 2010;40(3):586–592.
11. Heck DH, Zhao Y, Roy S, LeDoux MS, Reiter LT. Analysis of cerebellar function in Ube3a-deficient mice reveals novel genotype-specific behaviors. *Hum Mol Genet*. 2008;17(14):2181–2189.
12. Jiang YH, et al. Altered ultrasonic vocalization and impaired learning and memory in Angelman syndrome mouse model with a large maternal deletion from Ube3a to Gabrb3. *PLoS One*. 2010;5(8):e12278.
13. Sun J, Liu Y, Moreno S, Baudry M, Bi X. Imbalanced mechanistic target of rapamycin C1 and C2 activity in the cerebellum of Angelman syndrome mice impairs motor function. *J Neurosci*. 2015;35(11):4706–4718.
14. Brooks SP, Dunnett SB. Tests to assess motor phenotype in mice: a user's guide. *Nat Rev Neurosci*. 2009;10(7):519–529.
15. Albrecht U, et al. Imprinted expression of the murine Angelman syndrome gene, Ube3a, in hippocampal and Purkinje neurons. *Nat Genet*. 1997;17(1):75–78.
16. Gustin RM, et al. Tissue-specific variation of Ube3a protein expression in rodents and in a mouse model of Angelman syndrome. *Neurobiol Dis*. 2010;39(3):283–291.
17. Dindot SV, Antalffy BA, Bhattacharjee MB, Beaudet AL. The Angelman syndrome ubiquitin ligase localizes to the synapse and nucleus, and maternal deficiency results in abnormal dendritic spine morphology. *Hum Mol Genet*. 2008;17(1):111–118.
18. Judson MC, Sosa-Pagan JO, Del Cid WA, Han JE, Philpot BD. Allelic specificity of Ube3a expression in the mouse brain during postnatal development. *J Comp Neurol*. 2014;522(8):1874–1896.
19. Chamberlain SJ, Lalande M. Neurodevelopmental disorders involving genomic imprinting at human chromosome 15q11-q13. *Neurobiol Dis*. 2010;39(1):13–20.
20. Kishino T, Lalande M, Wagstaff J. UBE3A/E6-AP mutations cause Angelman syndrome. *Nat Genet*. 1997;15(1):70–73.
21. Lalande M, Calciano MA. Molecular epigenetics of Angelman syndrome. *Cell Mol Life Sci*. 2007;64(7–8):947–960.
22. Landers M, Calciano MA, Colosi D, Glatt-Deeley H, Wagstaff J, Lalande M. Maternal disruption of Ube3a leads to increased expression of Ube3a-ATS in trans. *Nucleic Acids Res*. 2005;33(13):3976–3984.
23. Zeilhofer HU, et al. Glycinergic neurons expressing enhanced green fluorescent protein in bacterial artificial chromosome transgenic mice. *J Comp Neurol*. 2005;482(2):123–141.
24. Ito M. Cerebellar control of the vestibulo-ocular reflex — around the flocculus hypothesis. *Annu Rev Neurosci*. 1982;5:275–296.
25. Nagao S. Role of cerebellar flocculus in adaptive interaction between optokinetic eye movement response and vestibulo-ocular reflex in pigmented rabbits. *Exp Brain Res*. 1989;77(3):541–551.
26. Wulff P, et al. Synaptic inhibition of Purkinje cells mediates consolidation of vestibulo-cerebellar motor learning. *Nat Neurosci*. 2009;12(8):1042–1049.
27. Schonewille M, et al. Purkinje cell-specific knockout of the protein phosphatase PP2B impairs potentiation and cerebellar motor learning. *Neuron*. 2010;67(4):618–628.
28. de Jeu M, De Zeeuw CI. Video-oculography in mice. *J Vis Exp*. 2012;(65):e3971.
29. Gao Z, van Beugen BJ, De Zeeuw CI. Distributed synergistic plasticity and cerebellar learning. *Nat*

Rev Neurosci. 2012;13(9):619–635.
30. Armstrong DM, Rawson JA. Activity patterns of cerebellar cortical neurones and climbing fibre afferents in the awake cat. *J Physiol*. 1979;289:425–448.
31. Marr D. A theory of cerebellar cortex. *J Physiol*. 1969;202(2):437–470.
32. De Zeeuw CI, Hoebeek FE, Bosman LW, Schonewille M, Witter L, Koekkoek SK. Spatiotemporal firing patterns in the cerebellum. *Nat Rev Neurosci*. 2011;12(6):327–344.
33. Hoebeek FE, et al. Increased noise level of purkinje cell activities minimizes impact of their modulation during sensorimotor control. *Neuron*. 2005;45(6):953–965.
34. Clopath C, Badura A, De Zeeuw CI, Brunel N. A cerebellar learning model of vestibulo-ocular reflex adaptation in wild-type and mutant mice. *J Neurosci*. 2014;34(21):7203–7215.
35. Cheron G, Servais L, Wagstaff J, Dan B. Fast cerebellar oscillation associated with ataxia in a mouse model of Angelman syndrome. *Neuroscience*. 2005;130(3):631–637.
36. Dieudonne S. Glycinergic synaptic currents in Golgi cells of the rat cerebellum. *Proc Natl Acad Sci U S A*. 1995;92(5):1441–1445.
37. Egawa K, et al. Decreased tonic inhibition in cerebellar granule cells causes motor dysfunction in a mouse model of Angelman syndrome. *Sci Transl Med*. 2012;4(163):163ra57.
38. Seja P, et al. Raising cytosolic Cl(–) in cerebellar granule cells affects their excitability and vestibulo-ocular learning. *EMBO J*. 2012;31(5):1217–1230.
39. Barski JJ, Dethleffsen K, Meyer M. Cre recombinase expression in cerebellar Purkinje cells. *Genesis*. 2000;28(3–4):93–98.
40. Weeber EJ, et al. Derangements of hippocampal calcium/calmodulin-dependent protein kinase II in a mouse model for Angelman mental retardation syndrome. *J Neurosci*. 2003;23(7):2634–2644.
41. Elgersma Y, et al. Inhibitory autophosphorylation of CaMKII controls PSD association, plasticity, and learning. *Neuron*. 2002;36(3):493–505.
42. Hansel C, et al. αCaMKII Is essential for cerebellar LTD and motor learning. *Neuron*. 2006;51(6):835–843.
43. van Woerden GM, et al. βCaMKII Controls the direction of plasticity at parallel fiber-Purkinje cell synapses. *Nat Neurosci*. 2009;12(7):823–825.
44. Silva-Santos S, et al. Ube3a reinstatement identifies distinct developmental windows in a murine Angelman syndrome model. *J Clin Invest*. 2015;125(5):2069–2076.
45. Galliano E, et al. Silencing the majority of cerebellar granule cells uncovers their essential role in motor learning and consolidation. *Cell Rep*. 2013;3(4):1239–1251.
46. Watanabe D, et al. Ablation of cerebellar Golgi cells disrupts synaptic integration involving GABA inhibition and NMDA receptor activation in motor coordination. *Cell*. 1998;95(1):17–27.
47. Riday TT, et al. Pathway-specific dopaminergic deficits in a mouse model of Angelman syndrome. *J Clin Invest*. 2012;122(12):4544–4554.
48. Farook MF, DeCuypere M, Hyland K, Takumi T, LeDoux MS, Reiter LT. Altered serotonin, dopamine and norepinepherine levels in 15q duplication and Angelman syndrome mouse models. *PLoS One*. 2012;7(8):e43030.
49. Fog JU, et al. Calmodulin kinase II interacts with the dopamine transporter C terminus to regulate amphetamine-induced reverse transport. *Neuron*. 2006;51(4):417–429.
50. Padmanabhan S, Lambert NA, Prasad BM. Activity-dependent regulation of the dopamine transporter is mediated by Ca(2+)/calmodulin-dependent protein kinase signaling. *Eur J Neurosci*. 2008;28(10):2017–2027.
51. Liu XY, et al. Activity-dependent modulation of limbic dopamine D3 receptors by CaMKII. *Neuron*. 2009;61(3):425–438.
52. Goossens HH, et al. Simple spike and complex spike activity of floccular Purkinje cells during the optokinetic reflex in mice lacking cerebellar long-term depression. *Eur J Neurosci*. 2004;19(3):687–697.
53. Zhou H, Voges K, Lin Z, Ju C, Schonewille M. Differential Purkinje cell simple spike activity and pausing behavior related to cerebellar modules. *J Physiol*. 2015;113(7):2524–2536.